PCCP

Accepted Manuscript

ROYAL SOCIETY OF CHEMISTRY

www.rsc.org/pccp

Unusual Photoluminescent Properties of the 3D Mixed-Lanthanide-Organic Frameworks Induced by Dimeric Structure: A Theoretical and Experimental Approach

Carime V. Rodrigues,[a] Leonis L. Luz,[b] José Diogo L. Dutra,[c] Severino A. Junior,[b] Oscar L. Malta,[b] Claudia C. Gatto,[a] Huayna C. Streit,[d] Ricardo O. Freire,*[c] Claudia Wickleder,*[d] and Marcelo Oliveira Rodrigues*[a]

[a] Instituto de Química, Campus Universitário Darcy Ribeiro, CEP 70904970, P.O.Box 4478, Brasilia-DF, Brazil.
[b] Departamento de Química Fundamental, UFPE, 50590-470, Recife - PE, Brazil.
[c] Pople Computational Chemistry Laboratory, Departamento de Química, Universidade Federal de Sergipe, 49100-000, São Cristóvão, Sergipe, Brazil.
[d] Inorganic Chemistry, Department of Science and Technology, University of Siegen. Adolf-Reichwein-Strasse 2, 57068 Siegen, Germany.

Keywords. lanthanides, luminescence, metal-organic framework, energy transfer.

Abstract. The present work describes a complementary experimental and theoretical investigation of the spectroscopic properties of the four isostructural 3D LnMOFs (wherein PDC = Pyrazole-3,5-dicarboxylate, $[La_2(PDC)_3(H_2O)_4]$ •$2H_2O$ **(1)**, $[(La_{0.9}Eu_{0.1})_2(PDC)_3(H_2O)_4]$ •$2H_2O$ **(2)**, $[(La_{0.9}Tb_{0.1})_2(PDC)_3(H_2O)_4]$ •$2H_2O$ **(3)** and $[(La_{0.9}Eu_{0.5}Tb_{0.5})_2(PDC)_3(H_2O)_4]$ •$2H_2O$ **(4))**. The experimental data and theoretical calculations show that the singular photophysical properties presented by these LnMOFs are induced by strong interaction between the Ln^{3+} ions.

INTRODUCTION

The potentialities of Metal-Organic Frameworks (MOF) to act as emissive materials have been intensively investigated in the past few years. This worldwide interest is justified by the fact that MOFs present excellent degree of structural predictability and a well-defined chemical environment, offered to organic groups and metal centers. The structural predictability allows the generation of numerous optical phenomenon, uncommon in conventional inorganic light-emitting materials.[1, 2] Among hundreds of luminescent CPs reported hiterto, uquestionably, CPs based on lanthanide ions, Lanthanide-Organic Frameworks (LnMOFs), may be considerd as the most promising due to the well-known

spectroscopic properties. These materials combine fairly interesting structures, thermodynamic stability, and well-established spectroscopic properties of Ln^{3+} ions. Moreover, they may undertake a multifunctional role by combining their optical, magnetic and structural properties for applications as sensors,[3-5] multimodal imaging agents [6] as well as gunshot residue (GSR) markers. [7, 8] Although a large number of works have been published in this field, [9-11] the development of luminescent LnMOFs is still in early stages, since the data presented by most of these reports are limited to the measurement of luminescence spectra, while detailed spectroscopic investigations together with theoretical calculations are still scarce.

The Stark structure and relative intensities of $^5D_0 \rightarrow {}^7F_J$ transitions have been widely used as optical probe to investigate the coordination environments of the Eu^{3+} ion in various materials for decades.[12, 13] In terms of Eu^{3+} coordination compounds, the majority of the published works have described spectral profiles typical of non-centro-symmetric compounds. Moreover, the hypersensitive transitions are dominant, and even for Eu^{3+} inserted in inorganic hosts, the majority of the luminescence spectra can be systematically well explained using a standard model of free ion (FI) with crystal-field (CF) interactions.[12] Unusual luminescence is generally produced, when the Eu^{3+} ion is located in an unusual lattice position.[13, 14] Some europium compounds derived from carboxylatodibenzoylmethanes exhibit anomalies in the Stark structure of their luminescence spectra, due to the influence of the nature of the substituent in the carboxylate unit.[14] Rocha *et al.* reported two examples of the microporous Eu-silicates, which display singular optical behaviors.[15] The $Na_3[(Y_{1-a}Eu_a)Si_3O_9]\bullet 3H_2O$, for example, permit an unusual detection of enantiomeric domains by use of unpolarized photoluminescence spectroscopy without the assistance of an external magnetic field.[15]

In this paper we wish to report an experimental and theoretical investigation of the unusual photoluminescence, $Ln^{3+} \rightarrow Ln^{3+}$ energy transfer (ET) and color tuning of the four isostructural 3D LnMOFs, $[La_2(PDC)_3(H_2O)_4]\bullet 2H_2O]$, $[(La_{0.9}Eu_{0.1})_2(PDC)_3(H_2O)_4]\bullet 2H_2O$,

$[(La_{0.9}Tb_{0.1})_2(PDC)_3(H_2O)_4]\bullet 2H_2O$, and $[(La_{0.9}Eu_{0.05}Tb_{0.05})_2(PDC)_3(H_2O)_4]\bullet 2H_2O$, herein designated as **(1)** to **(4)**, respectively (where PDC corresponds to Pyrazole-3,5-dicarboxylate).

RESULTS AND DISCUSSION

Previous works have reported LnMOFs based on pyrazole-3,5-dicarboxylate (PDC) ligands.[16,17] The single-crystal X-ray diffraction investigations unequivocally reveal that **(1)-(4)** display 3D structures and crystallize in the monoclinic space group Cc (Table 1S), identical to previous reports.[17, 18] Each asymmetric unit of **(1)** comprises two crystallographically independent La^{3+} ions, three PDC^{2-} ligands, four coordinated water molecules, and two lattice water molecules (Figure 1 (a)). La(1) is coordinated by three nitrogen atoms from pyrazole rings, six oxygen atoms from carboxylate of PDC^{2-} ligands, $\{LaN_3O_6\}$, while La(2) is bonded to five oxygen atoms from carboxylate groups and four other ones from coordinated water molecules, $\{LaO_9\}$. Hence, these coordination polyhedra may be described as monocapped square antiprisms, highly distorted from the ideal symmetry C_{4v}, (Figure 1(b)). The crystallographically independent La^{3+} ions are interconnected by carboxylate groups of the adjacent PDC^{2-} residues, which adopt four distinct coordination fashions (unidentate, bridging-chelating, *syn-syn* bridge and $\mu_{1,1}$-oxo-bridge). This results in a 3D framework, in which the La(1)•••La(2) separation is 4.07Å. This distance is shorter than in other La···La complexes with corresponding distances between 4.105(1) and 5.413(1) Å.[19] The resulting framework presents one-dimensional channels running along to *c* axis formed by fused four-membered rings (Figure 1(c)).

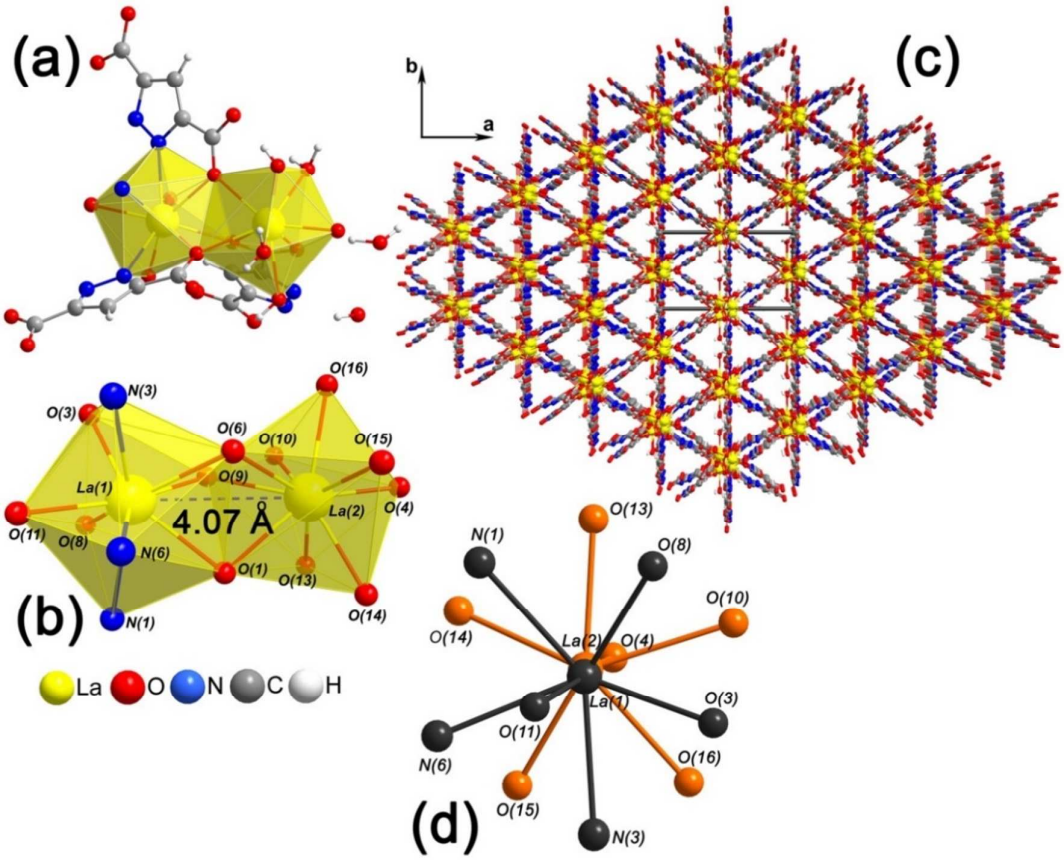

Figure 1. (a): Asymmetric unit of **(1)**; (b): Schematic representation of monocapped square antiprisms coordination polyhedrons of the La^{3+}dimer, emphasizing the La(1)•••La(2) distance; (c): View along of c axis of the extended structure of **(1)**, displaying the distorted 4-membered channels; (d): Representation eclipsed of atoms in opposite spatial positioning. $\{LaN_3O_6\}$ and $\{LaO_9\}$ sites are represented in dark grey and orange, respectively. O(1), O(6) and (9) were omitted for clarity.

Figure 2 exhibits the excitation spectrum of **(2)** acquired in the 240-600 nm spectral range at room temperature, while monitoring the Eu^{3+} $^5D_0 \rightarrow {}^7F_2$ emission at 611 nm.

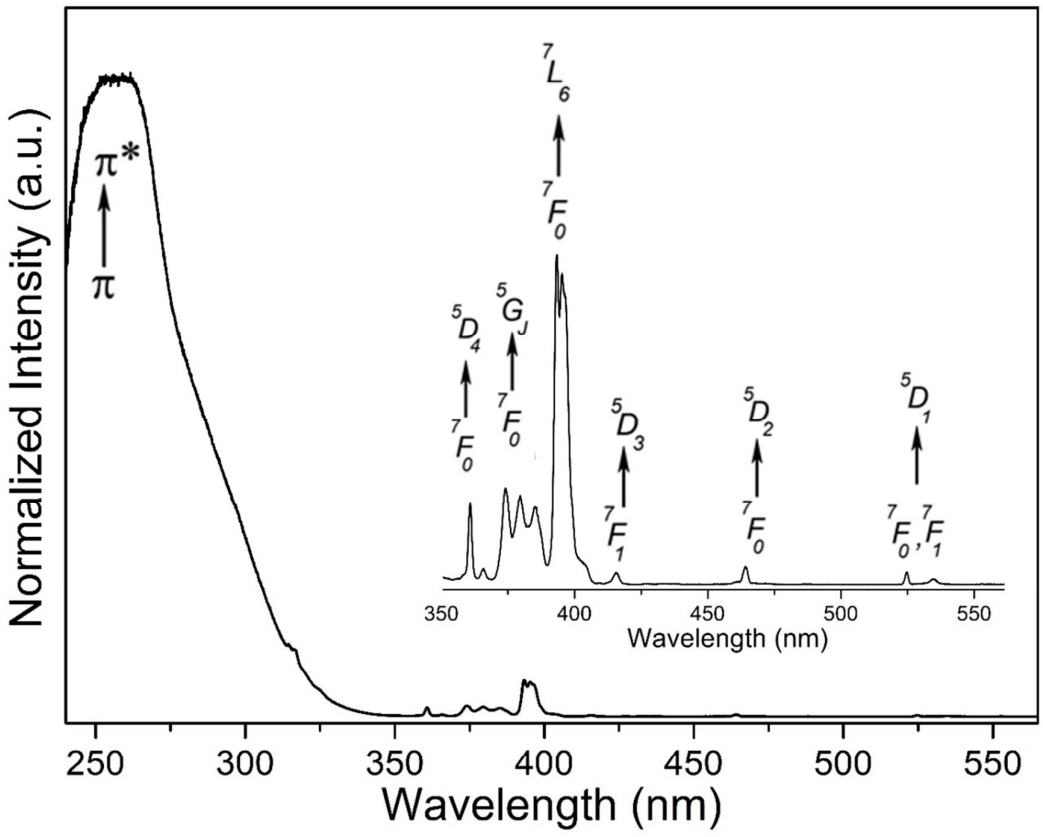

Figure 2. Excitation spectrum of **(2)** measured at room temperature, by monitoring the Eu^{3+} emission at 591 nm. Inset: Spectrum expanded in the *4f—4f* region.

The excitation spectrum of **(2)** displays an intense broad band centered at ca. 260 nm, assigned to the $\pi \rightarrow \pi^*$ electronic transition of the PDC^{2-} residues. Very weak peaks are observed between 350 and 550 nm, arising from the *4f—4f* transitions, typical of the Eu^{3+} ion. This spectral profile indicates that $\pi \rightarrow \pi^*$ excitation followed by intramolecular energy transfer is the most effective excitation pathway responsible for the orange color emission presented by the LnMOF material.

The emission spectrum of **(2)** measured at room temperature upon excitation at *ca.* 280 nm is depicted in Figure 3.

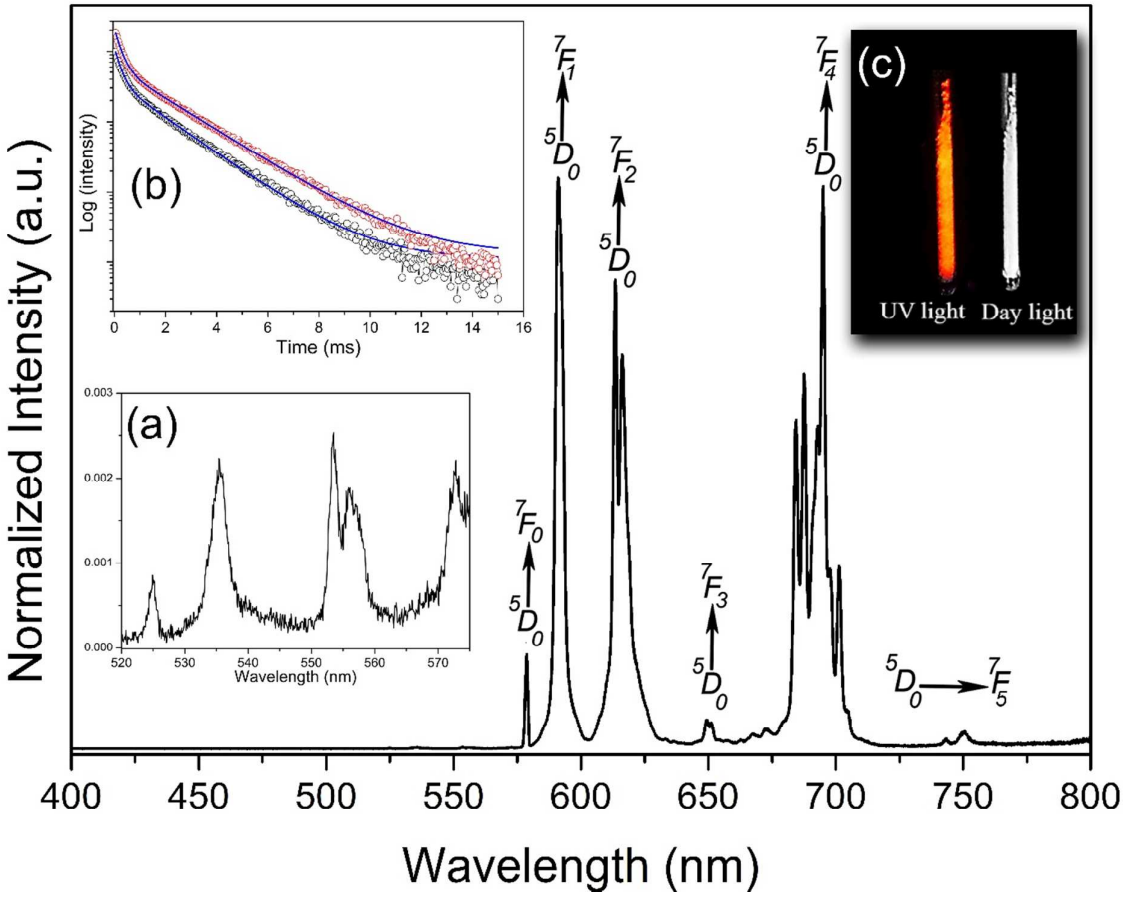

Figure 3. Emission spectrum of **(2)** acquired at room temperature upon excitation at 260 nm. Inset: (a) Steady-state emission spectrum expanded in the $^5D_1 \rightarrow {}^7F_j$ region; (b) Decay emission curves obtained at 10K (black circle) and 330K (red circle) upon excitation at 395 nm, while monitoring the $^5D0 \rightarrow {}^7F_2$ transition. The blue solid lines represent the best fit. Inset: Sample under UV irradiation and day light.

The spectra are composed by narrow bands characteristic of the Eu^{3+} $^5D_0 \rightarrow {}^7F_J$ transitions, those attributed to the $^5D_0 \rightarrow {}^7F_1$, $^5D_0 \rightarrow {}^7F_2$ and $^5D_0 \rightarrow {}^7F_4$ transitions give the major contribution to the photoluminescence of the material (Inset Figure 3). The Eu^{3+} emission lines are normally employed as probes to investigate the coordination environment around the ion. In fact, the Eu^{3+} $^5D_0$ and ^7F_J states are weakly affected by the ligand field, whereas the relative intensities and splitting of the transitions involving the $^{2S+1}L_J$ multiplets with $J > 0$ are symmetry-dependent. The transitions $^5D_0 \rightarrow {}^7F_J$ (J = 0, 3, 5), forbidden by the magnetic dipole, forced electric dipole and dynamic coupling mechanisms, may be observed in the emission spectra of **(2)** due to J-mixing effects. The hypersensitive transition, $^5D_0 \rightarrow {}^7F_2$, presents two well defined peaks centered at 614 and 616 nm, while the $^5D_0 \rightarrow {}^7F_1$, which is

governed by the magnetic dipole mechanism and is quite independent of ligand field effects, exhibits one well defined Stark level centered at *ca.* 592 nm. The emission spectrum of **(2)** presents a peak centered at *ca.* 579 nm with full width at half maximum (FWHM) of 50 cm^{-1}, assigned to the $^5D_0 \rightarrow {}^7F_0$ transition. Although this transition is forbbiden by forced electric dipole mechanism, its presence in emission spectra may be attributed to the *J*-mixing of $^7F_0$ with $^7F_2$, $^7F_4$ and $^7F_6$ states.[20-22] The mechanism proposed by Wybourne *et al.* describes the contribution spin–orbit interaction between the states of an intermediate excited configuration, which induce violation of the ΔS and ΔJ selection rules.[23] From the point group selection rule, the the $^5D_0 \rightarrow {}^7F_0$ transition is allowed when the coordination site presents a local symmetry of the type C_s, C_n or C_{nv}.[24] The lifetime curves of **(2)** acquired at 10 K and room temperature (Figure 3 (b)) upon excitation at 395 nm while monitoring $^5D_0 \rightarrow {}^7F_2$ at 614 nm, display a bi-exponential profiles with lifetimes of 1.93 ± 0.008 and 0.25 ± 0.001 nm, and 1.70 ± 0.010 ms and 0.23 ± 0.002, respectively. As well-stablished that the O—H oscillators are the most effective quenchers of the Eu^{3+} excitated states and only the Ln(2) site has presented four water molecules directly coordinated to Eu^{3+} ion, hence, these non-exponentional behaviors may be assigned to the emission of Eu^{3+} ions situated at Ln(1) and Ln(2) sites respectively.

Figure 4 displays the expanded regions of the emission spectra of **(2)** measured at 10, 25 and 300K.

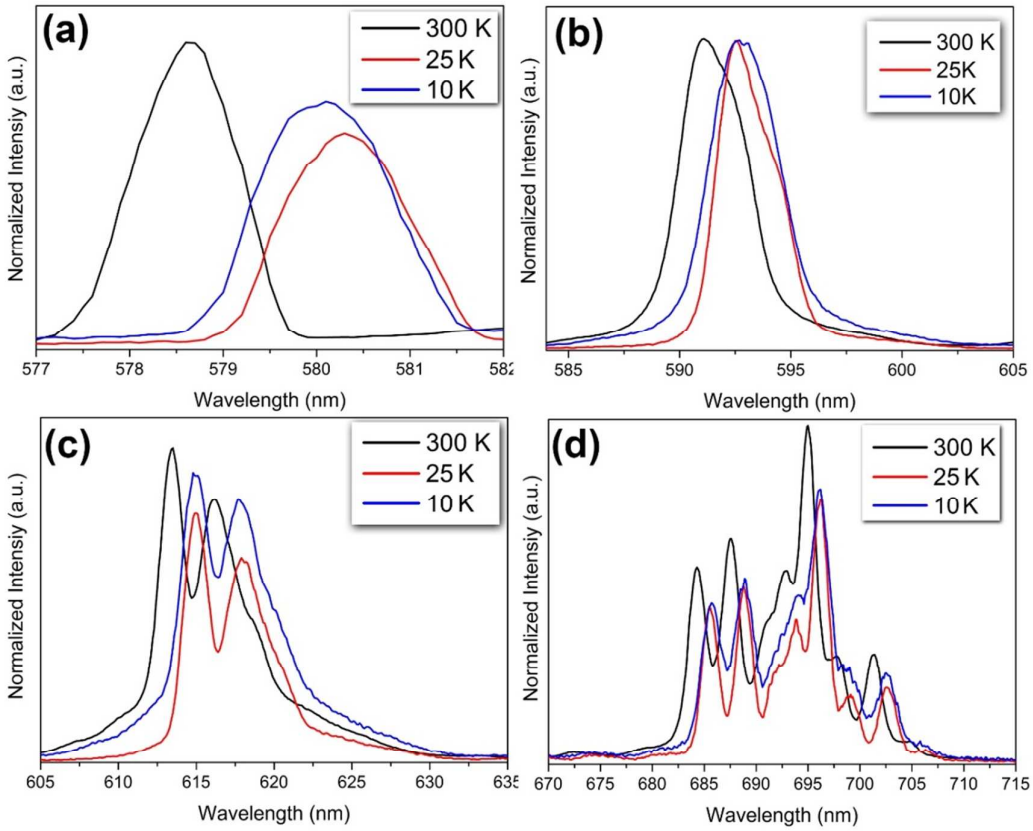

Figure .4 Emission spectra of **(2)** acquired at 10, 25 and 398 K upon excitation at 395 nm and expanded in transition regions: (a) $^5D_1 \rightarrow {}^7F_0$; (b) $^5D_1 \rightarrow {}^7F_1$;(c) $^5D_1 \rightarrow {}^7F_{2B;}$ (d) $^5D_1 \rightarrow {}^7F_4$.

The expanded spectra show no changes in the Stark splitting on decreasing the temperature, which may be justified by a strong Ln(1)─Ln(2) interaction. The uncommon high intensity of $^5D_0 \rightarrow {}^7F_4$ transition relative to magnetic dipole-allowed $^5D_0 \rightarrow {}^7F_1$ transition is an indicative that the local symmetry group of Ln(1)─Ln(2) dimer toward an high symmetric environment.[25] In accordance with the crystallographic investigations, the Ln^{3+} polyhedra are connected via two $\mu_{1,1}$-oxo-bridging oxygen atoms from carboxylates groups of the PDC^{2-} ligands, forming a highly symmetric binuclear structure, (Figure 1(b)). As illustrated in Figure 2 (d), the pair of atoms Ln(1):Ln(2), O(4):O(11), O(8):O(15), O(3):O(14), N(1): O(16), N(3):O(13) and N(6):O(10) are in opposite spatial positions across the *pseudo* inversion center localized between the Ln^{3+} ions. The relative intensities and lack of additional splitting of the Eu^{3+} transitions at low temperature constitute to an unusual spectral structure in comparison with most other MOFs and complexes based on Ln^{3+}—Ln^{3+} dimers

reported hitherto.[5, 26-29] In comparison with previous reports that have described the spectroscopic properties of LnMOFs containing dimeric structures, the results presented here may be considered as interesting, since, according to our theoretical results discussed below, neither Eu(1) nor Eu(2) could, isolated, produce an emission spectra with this profile. Férey *et. al* have reported an investigation of the spectroscopic properties of the EuBDC material which presents a dimeric structure composed by seven and eight-coordinated of Eu^{3+} sites.[5] Férey has shown that even at 10K, the time-resolved spectra under selective excitation in both $^5D_0 \rightarrow {}^7F_0$ transitions of EuBDC the emission spectrum from individual sites cannot be recorded independently from each other at longer delay times. In addition, the short Eu^{3+}—Eu^{3+} distance (4.725 Å) and the strong interactions corroborated with the observation of the up-converted Eu^{3+} emission in EuBDC material.[5] Ananias *et al.* described the most iconic example of the effect of dimeric structure on optical properties of a Eu^{3+}-containing zeolite. $K_7[(Eu_3)Si_{12}O_{32}]\bullet 4H_2O$ presents a centrosymmetric Eu^{3+}–Eu^{3+} dimer whose the intermetallic distance is 3.87 Å and another isolated Eu^{3+} ion inserted in a distorted octahedral geometry. [30] In this system the experimental and theoretical evidences indicate that due to the short intermetallic distance the Eu^{3+}–Eu^{3+} dimer behaves like a single entity. The interaction between the isolated Eu^{3+} ion and the Eu^{3+}–Eu^{3+} dimer in $K_7[(Eu_3)Si_{12}O_{32}]\bullet 4H_2O$ results an atypical long lifetime (10.3 ms) and a singular emission signature.

The intensity parameters Ω_λ (λ= 2, 4 and 6), as defined in Equations **1** and **2**, derived from the Judd-Ofelt theory can give us information on the strength of all *4f – 4f* transitions allowed by the forced electric dipole and dynamic coupling mechanisms. Theoretically, these parameters have been calculated by adjusting the charge factors (g) and polarizabilities (α), appearing in Equations **3** and **4**, respectively, to reproduce the phenomenological (experimental) values of the Ω_2 and Ω_4 parameters.[19, 31-33]

$$\Omega_{\lambda} = (2\lambda+1)\sum_{t}^{\lambda-1,\lambda+1(odd)}\sum_{p=0}^{t(all)}\frac{\left|B_{\lambda tp}\right|^2}{(2t+1)} \quad (1)$$

$$B_{\lambda tp} = \frac{2}{\Delta E}\left\langle r^{t+1}\right\rangle\theta(t,p)\gamma_p^t - \left[\frac{(\lambda+1)(2\lambda+3)}{2\lambda+1}\right]\left\langle r^{\lambda}\right\rangle(1-\sigma_{\lambda})\left\langle f\left\|C^{(\lambda)}\right\|f\right\rangle\Gamma_p^t\delta_{t,\lambda+1} \quad (2)$$

$$\gamma_p^t = \left(\frac{4\pi}{2t+1}\right)^{1/2} e^2\sum_j \rho_j\left(2\beta_j\right)^{t+1}\frac{g_j}{R_j^{t+1}}Y_p^{t*}\left(\theta_j,\varphi_j\right) \quad (3)$$

$$\Gamma_p^t = \left(\frac{4\pi}{2t+1}\right)^{1/2}\sum_j \frac{\alpha_j}{R_j^{t+1}}Y_p^{t*}\left(\theta_j,\varphi_j\right) \quad (4)$$

Differently from the usual spectral behaviors presented by most of the Eu^{3+}-based materials, the experimental intensity parameters obtained from the emission spectrum are related with the dimeric structure, represented by the coordination environment of the Ln(1)─Ln(2) dimer. The solution of this singular problem arises from a theoretical methodology named "*Overlapped Polyhedra Method*" (*OPM*).[34] This new approach consists in adjusting the charge factors (g) and polarizabilities (α), associated with all coordinated atoms for both europium ions, considering as center of the system the two overlapped europium centers. The angular adjustment is performed guaranteeing the overlap of three common oxygen atoms (O(1), O(6) and O(9)) for both polyhedra. The values of g and α calculated from overlapped sites were applied for each isolated polyhedron. It is important to make it clear that these results simulate the individual spectroscopic properties of the moiety Eu(1) and Eu(2) sites. The coordination polyhedra calculated from Sparkle/PM3[35] are displayed in Figure 2S (see Supporting Information).

Tables 1 and 2 collect the theoretical spherical coordinates, charge factors (g) and the polarizabilities (α) calculated for the polyhedra $\{EuN_3O_6\}$ and $\{EuO_9\}$ respectively, while Table 3 presents the experimental and calculated intensity parameters, radiative (A_{rad}) and nonradiative (A_{nrad}) decay rates and quantum yields (*q*) obtained for each coordination polyhedron via the *Overlapped Polyhedra Method*.

Table 1: Spherical Atomic Coordinates for the Sparkle/PM3 {EuN_3O_6} polyhedron of **(2)**, charge factors (g) and polarizabilities (α in cm^3) of the coordinated atoms.

Atom	*R/Å*	θ/°	ϕ/°	*g*[a]	α[a]
O(1)	2.50185	72.546	299.174	0.1104	4.1806×10^{-24}
O(3)	2.45955	147.467	216.593	0.0584	5.0057×10^{-24}
O(6)	2.46619	65.032	231.682	0.1104	4.1806×10^{-24}
O(8)	2.46246	95.504	154.553	0.0584	5.0057×10^{-24}
O(9)	2.51008	3.538	274.665	0.1104	4.1806×10^{-24}
O(11)	2.48017	126.171	69.156	0.0584	5.0057×10^{-24}
N(1)	2.52510	59.339	97.085	0.3020	2.6313×10^{-24}
N(3)	2.53595	129.320	330.227	0.3020	2.6313×10^{-24}
N(6)	2.56034	81.164	24.096	0.3020	2.6313×10^{-24}

[a] Obtained using a *Overlapped Polyhedra Method*.

Table 2: Spherical Atomic Coordinates for the Sparkle/PM3 {EuO_9} polyhedron of **(2)**, charge factors (g) and the polarizabilities (α in cm^3) of the coordinated atoms.

Atom	*R/Å*	θ/°	ϕ/°	*g*[a]	α[a]
O(1)	2.46963	147.888	23.216	0.1104	4.1806×10^{-24}
O(4)	2.44423	43.869	263.471	0.0584	5.0057×10^{-24}
O(6)	2.40128	138.599	147.754	0.1104	4.1806×10^{-24}
O(9)	2.47071	97.837	88.696	0.1104	4.1806×10^{-24}
O(10)	2.39908	99.491	192.325	1.8648	1.5190×10^{-24}
O(13)	2.47162	43.485	148.267	1.1194	3.3031×10^{-24}
O(14)	2.50068	41.142	38.034	1.1194	3.3031×10^{-24}
O(15)	2.46234	83.574	326.411	1.1194	3.3031×10^{-24}
O(16)	2.46780	119.890	265.316	1.1194	3.3031×10^{-24}

[a] Obtained using a *Overlapped Polyhedra Method*.

Table 3. Experimental and theoretical intensity parameters from *OPM*, radiative and non-radiative decay rates (A_{rad} and A_{nrad}),) and absolute quantum yields (q).

	Experimental	**Overlapped Polyhedra Method (*OPM*)**	
		{EuN_3O_6}	**{EuO_9}**
Ω_2 (x 10^{-20} cm^2)	2.1	2.01	3.76
Ω_4 (x 10^{-20} cm^2)	5.1	1.06	3.17
Ω_6 (x 10^{-20} cm^2)	-	0.65	0.17
A_{rad} (s^{-1})	190	127.0	211.5
A_{nrad} (s^{-1})	-	642.4	3955.2
q (%)	42%	16.3	5.00

The values obtained via "*Overlapped Polyhedra Method"* for charge factors (g) presented in Tables 1 and 2, are similar to those ones previously reported for europium materials.[36, 37] The theoretical values of intensity parameters, summarized in Table 3, are in good agreement with those obtained experimentally for dimeric structure. The value of Ω_4 parameter is higher than one exhibited by Ω_2, suggesting that the chemical environment of the Eu^{3+} ion tends toward a high symmetry.[38] Nevertheless, the calculation of the intensity parameters by using *OPM* shows that both Eu^{3+} sites present higher Ω_2 values than the Ω_4 ones. These results indicate a spectral dominance of the hypersensitive transition as typically observed in nine-fold coordinated Eu^{3+} MOFs and complexes.[27, 39-43] The standard 4*f*–4*f* intensity theory indicates that when the coordination polyhedron tends towards a much higher symmetry the higher odd-rank γ_p^5 and Γ_p^5 are dominant, leading to an increasing of Ω_4 and a decreasing of Ω_2. [38, 44] When the chemical environment of the Eu^{3+} ion tends towards a much distorted coordination geometry, then the lower odd-rank components γ_p^t and Γ_p^t (t =1 and 3) become preponderant, leading to a reduction in the value of Ω_4 while Ω_2 is increased.[44]

The average value of A_{rad} from both polyhedra (169.5 s^{-1}) is in good agreement to the experimental one supporting the hypothesis that the high interaction between the Ln^{3+} ions. The ligand triplet energy for Eu(1) and Eu(2) sites (Table 4) were estimated at 27163.6 and 18398.9 cm^{-1} (Table 3S) and provide a plausible explanation for the absolute quantum yield (q) of 42%.

Theoretical rates for a single Eu(1)↔Eu(2) energy transfer (ET) process as well as the contributions of dipole—dipole (*D*—*D*), dipole—quadrupole (*D*—*Q*), quadrupole — quadrupole (*Q*—*Q*) and exchange (*Ex*) mechanisms may be calculated by the methodology developed by one of us (OLM).[45] This method was developed in accordance with Kushida's

expressions (Equations **5**—**8**), which do not consider the shielding effects for the energy transfer mechanisms: [46-48]

$$W_{D-D} = \frac{(1-\sigma_1^D)^2(1-\sigma_1^A)^2}{\left[J_D^*\right]\left[J_A\right]}\frac{4\pi}{3\hbar}\frac{e^4}{R^6}\left(\sum_K \Omega_K^D \left\langle \psi_D J_D \left\| U^{(K)} \right\| \psi_D^* J_D^* \right\rangle^2\right) \times \left(\sum_K \Omega_K^A \left\langle \psi_A J_A \left\| U^{(K)} \right\| \psi_A^* J_A^* \right\rangle^2\right) F \quad (5)$$

$$W_{D-Q} = \frac{(1-\sigma_1^D)^2(1-\sigma_2^A)^2}{\left[J_D^*\right]\left[J_A\right]}\frac{2\pi}{\hbar}\frac{e^4}{R^8}\left(\sum_K \Omega_K^D \left\langle \psi_D J_D \left\| U^{(K)} \right\| \psi_D^* J_D^* \right\rangle^2\right) \times \left\langle r^2 \right\rangle_A^2 \left\langle f \left\| C^2 \right\| f \right\rangle^2 \times \left\langle \psi_A^* J_A^* \left\| U^{(2)} \right\| \psi_A J_A \right\rangle^2 F \quad (6)$$

$$W_{Q-Q} = \frac{(1-\sigma_2^D)^2(1-\sigma_2^A)^2}{\left[J_D^*\right]\left[J_A\right]}\frac{28\pi}{5\hbar}\frac{e^4}{R^{10}} \times \left\langle r^2 \right\rangle_D^2 \left\langle r^2 \right\rangle_A^2 \left\langle f \left\| C^2 \right\| f \right\rangle^4 \times \left\langle \psi_D J_D \left\| U^{(2)} \right\| \psi_D^* J_D^* \right\rangle^2 \times \left\langle \psi_A^* J_A^* \left\| U^{(2)} \right\| \psi_A J_A \right\rangle^2 F \quad (7)$$

$$W_{Ex} = \frac{\left\langle 4f \left| L \right| \right\rangle^4}{\left[J\right]}\frac{8\pi}{3\hbar}\frac{e^2}{R_l^4} \times \left\langle \psi^* J^* \left\| S \right\| \psi J \right\rangle^2 \times \sum_m \left| \phi \left\langle \sum_j \mu_z(j) S_m(j) \right| \phi^* \right\rangle \right|^2 F \quad (8)$$

where the *D* and *A* indexes represent donor and acceptor species, [*J*] is 2*J* +1, *R* is donor - acceptor distance, $\langle r^2 \rangle$ is a 4f radial integral, (1 - σ) are shielding factors of the lanthanide ions, $\left\langle \psi\ J \left\| U^{(k)} \right\| \psi^* J^* \right\rangle^2$ are squared reduced matrix elements, in the intermediate coupling scheme of the unit tensor operators $U^{(k)}$ and $\left\langle l \left\| C^{(\lambda)} \right\| l \right\rangle$ are reduced matrix elements of the Racah's tensor operators. σ_2, σ_4 and σ_6 values are determined from Edvardsson and Klintenberg, [49] σ_1 is calculated from Equation 9 of Ref.45 proposed by Malta[45]

$$(1-\sigma_k) = \rho(2\beta)^{k+1} \quad (9)$$

where β is a number very close to 1, ρ designates the radial overlap integral between the 4*f* sub-shell and the valence shell of a ligand atom in the first coordination sphere. In lanthanide compounds the typical value of ρ is 0.05.

The *F* values in Equations **5** to **8** arise from the overlap between the bands of donor emission and acceptor absorption. *F* may be estimated from Equation **10**. [50]

$$F = \frac{\ln 2}{\sqrt{\pi}} \frac{1}{\hbar^2 \gamma_D \gamma_A} \left\{ \left[\left(\frac{1}{\hbar\gamma_D} \right)^2 + \left(\frac{1}{\hbar\gamma_A} \right)^2 \right] \ln 2 \right\}^{-1/2} \times \exp\left\{ \frac{1}{4} \frac{\frac{2\Delta}{(h\gamma_D)^2} \ln 2}{\left[\left(\frac{1}{\hbar\gamma_A} \right)^2 + \left(\frac{1}{\hbar\gamma_D} \right)^2 \right] \ln 2} - \left[\frac{\Delta}{\hbar\gamma_D} \right]^2 \ln 2 \right\} \quad 10$$

where $\hbar\gamma$ corresponds to the band width at half-height and Δ is the energy gap between donor and acceptor. Typically, *F* values are in the 10^{-12} - 10^{-13} erg^{-1} range. All values for the numerical estimation of the energy transfer process between the two lanthanide ions are displayed in Table 4S (see Supporting Information).

The calculation considers R as the shortest Ln^{3+}—Ln^{3+} distances from the crystallographic structure, 4.07Å, and ET rate values for $Eu^{3+}(1) \rightarrow Eu^{3+}(2)$ ET processes are collected in Table 4.

Table 4. Calculated values of intramolecular energy transfer between $Eu^{3+}(1)$ and $Eu^{3+}(2)$ ions.

Mechanism	$Eu(^5D_0) \rightarrow Eu(^5D_0)$ (s^{-1})	$Eu(^5D_1) \rightarrow Eu(^5D_0)$ (s^{-1})
D—D	5.36×10^3	1.47×10^3
D—Q	1.18×10^4	3.25×10^3
Q—Q	4.88×10^4	1.59×10^4
Ex	1.42	1.17

The relatively high values of the $Eu^{3+}(1)\rightarrow Eu^{3+}(2)$ ET rates corroborate with a strong interaction between the $Eu^{3+}(1)$—$Eu^{3+}(2)$ pair. Considering the channels investigated, the ET processes are predominantly governed by the *D*—*Q* and *Q*—*Q* mechanisms.

In Figure 5, the excitation and emission spectra of **(3)** are depicted.

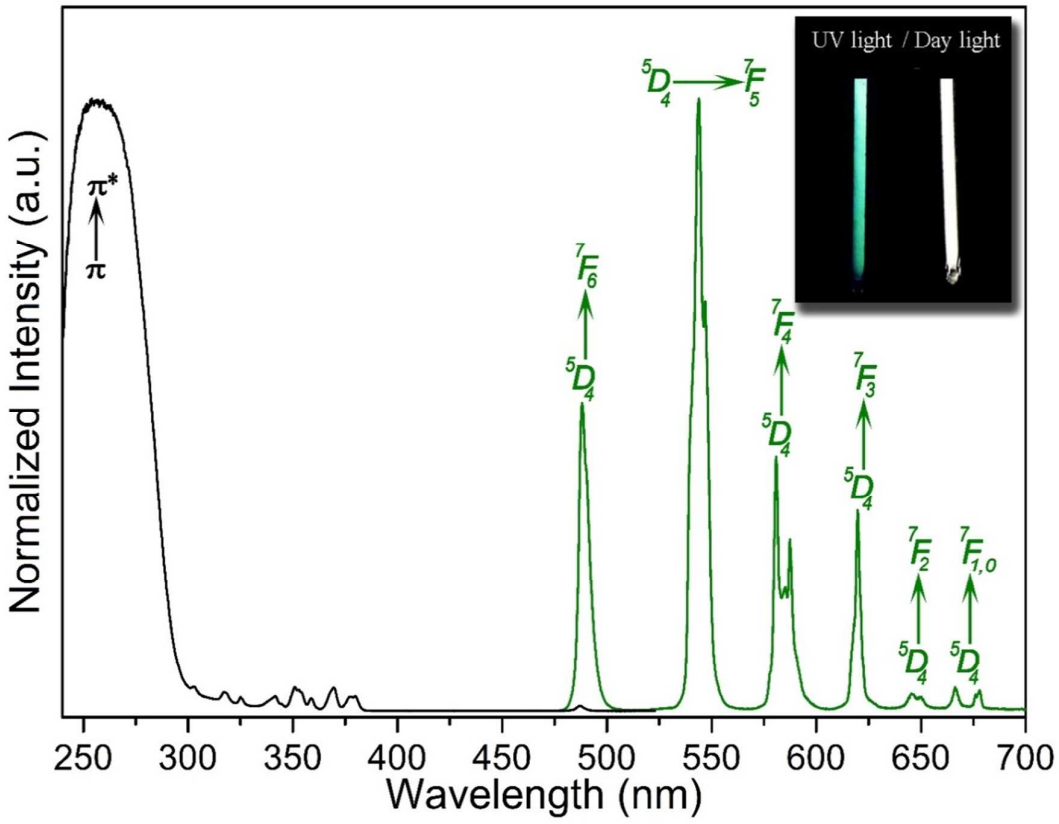

Figure 5. Excitation and emission spectra of **(3)** acquired at room temperature. Inset: Sample under UV irradiation and day light.

The excitation spectrum recorded from 240 to 520 nm, while monitoring the Tb^{3+} $^5D_4\rightarrow {}^7F_5$ transition at *ca.* 543 nm, displays a broad band with the same maximum observed for (2) at *ca.* 260 nm, typical for the $\pi\rightarrow\pi^*$ transition associated with the PDC^{2-} ligand. The weak sharp excitation signals observed in the 300-490 nm spectral range are attributed to the f - f transitions of Tb^{3+} ions. These results indicate that the indirect excitation of the emitting center followed by ligand-Tb energy transfer is the most efficient photophysical pathway responsible for the green emission of the sample. The emission spectrum of (3) exhibits

characteristic narrow bands of the Tb^{3+} $^5D_4 \rightarrow {}^7F_j$ transitions, among which $^5D_4 \rightarrow {}^7F_5$ is the most intense one and corresponds to 47% of the integrated emission spectrum. This transition presents simultaneously the largest contribution from the magnetic dipole and forced electric dipole mechanisms. The decay curve of the Tb^{3+} $^5D_4 \rightarrow {}^7F_5$ transition in (3) acquired at room temperature, displays a single exponential profile with emission lifetime (τ) of 1.78 ± 0.01 ms, even in the presence of two crystallographically independent Ln^{3+} sites. This result may be understood on the basis of a significant contribution of the magnetic dipole mechanism, which is quite independent on the chemical environment, to this transition of the Tb^{3+} ion.[41] As a consequence, the lifetimes of the Tb(1) and Tb(2) sites do not exhibit a distinguishable difference, justifying the lack of a nonexponetial behavior at short time domains. Compound (3) shows an absolute quantum yield of 14%, consistent with a rather low balance between absorption, intramolecular and ion – ion energy transfer, and decay rates in the MOF matrix.

The photoluminescence spectra of **(4)** measured at room temperature and the Commission International de l´Eclairage (CIE) chromaticity diagram [51] points are depicted in Figure 6.

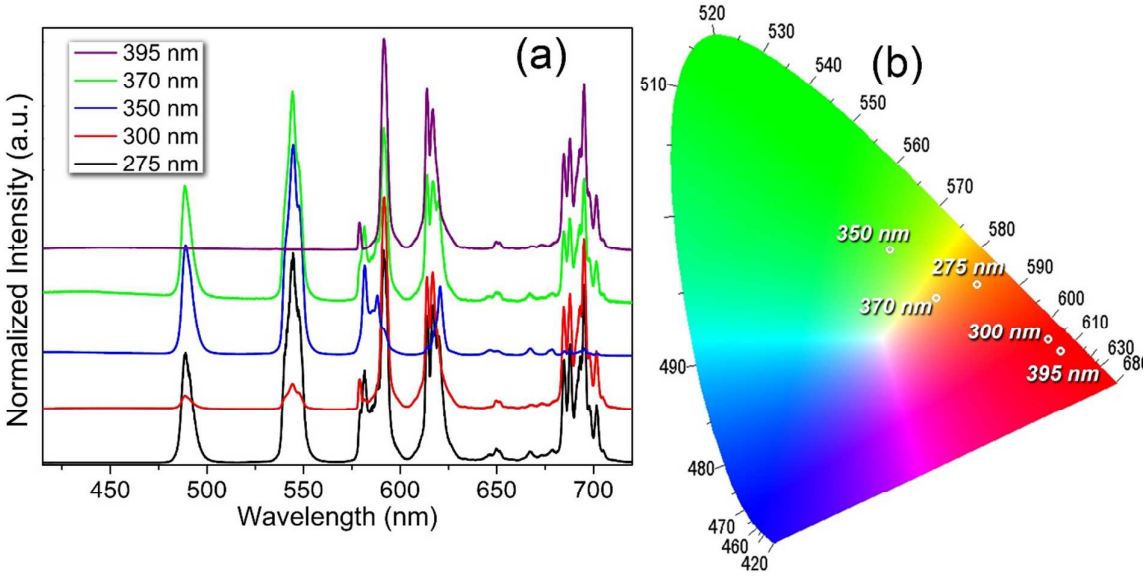

Figure 6. (a) Emission spectrum of **(4)** acquired at room temperature upon excitations at 275, 300, 350, 370 and 395 nm. (b) CIE diagram of **(4)** for different excitation wavelengths.

The fluorescence lifetimes give information about ET rates and efficiency of the Ln^{3+}—Ln^{3+} interaction. The $Tb^{3+}\rightarrow Eu^{3+}$ ET have influenced the luminescence decay profile of the donor species, Tb^{3+}, in comparison with that presented by **(3)**. In the case of slow donor—donor energy migration, it is expected that the decay curve of the donor presents a non-exponential behavior at short time domains, caused by direct ET from the donor to the nearest acceptor neighbors and an exponential component at long times due to energy diffusion among donors.[52, 53] The decay curve of the Tb^{3+} ion in **(4)** presents a non-exponential profile in short time domains with an average lifetime of (τ) of 0.30 ms, due to the direct ET from Tb^{3+} to the nearest Eu^{3+} ions, and a long monoexponential component with lifetime of (τ) of 1.98 ± 0.05 ms caused by energy migration among the donors and radiative decay from the $^5D_4$ level.

Considering that the effect of the lanthanide contraction is insignificant, the ET rate (k_{ET}), efficiency (η_{ET}) of the $Tb^{3+}\rightarrow Eu^{3+}$ ET process and the critical transfer distance were estimated by Equation **11**-**13**.[54, 55]

$$k_{ET} = \tau_1^{-1} - \tau_0^{-1} \qquad 11$$

$$\eta_{ET} = \frac{\tau_1^{-1} - \tau_0^{-1}}{\tau_1^{-1}} \qquad 12$$

$$k_{ET} = \tau_0^{-1}\left(\frac{R_0}{R}\right)^S \qquad 13$$

where R is the Ln^{3+} ions pair distance (4.07 Å), R_0 is the critical transfer distance and S= 6, 8, 10 for D—D, D—Q and Q—Q interactions. The k_{ET} and $\eta_{ET,}$ values are 2778 s^{-1} and 83%, while R_0 from Equation (13) are 5.30, 5.0 and 4.8 Å for D—D, D—Q and Q—Q mechanisms, respectively. These results demonstrate that the Tb^{3+} ion is enabled to transfer energy efficiently to the nearest Eu^{3+} cation. The Malta´s methodology was applied again to calculate

the single $Tb^{3+}\rightarrow Eu^{3+}$ energy transfer process by the mechanisms *D*—*D*, *D*—*Q*, *Q*—*Q* and *Ex*. The calculation considers the ET channels $Tb^{3+}/^5D_4\rightarrow Eu^{3+}/^5D_1$ and $Tb^{3+}/^5D_4\rightarrow Eu^{3+}/^5D_0$. ET rate values for a single $Tb^{3+}\rightarrow Eu^{3+}$ process (Table 5) indicate that the interactions are predominantly governed by *D*—*Q* and *Q*—*Q* mechanisms.

Table 5. Calculated values of intramolecular energy transfer between Tb^{3+} and Eu^{3+} ions.

Mechanism	$Tb(^5D_4) \rightarrow Eu(^5D_1)$ (s^{-1})	$Tb(^5D_4) \rightarrow Eu(^5D_0)$ (s^{-1})
D—D	170.142	297.62
D—Q	446.512	657.73
Q—Q	442.97	652.52
Ex	1.22	7.11

The emission spectra of mixed-lanthanide LnMOFs, Figure 5 (a), display characteristic narrow bands corresponding to the centered $Eu^{3+}\ ^5D_0\rightarrow ^7F_j$ and $Tb^{3+}\ ^5D_4\rightarrow ^7F_j$ transitions. Emission spectra of **(4)** has demonstrated sensible dependence on the excitation wavelength, since the relative intensities of the $Eu^{3+}\ ^5D_0\rightarrow ^7F_j$ and $Tb^{3+}\ ^5D_4\rightarrow ^7F_j$ transitions have been substantially changed upon distinct excitations, enabling an efficient tuning of the photoluminescence color. Upon excitation at 275 nm, **(4)** displays a quantum yield of 19%. The CIE diagram, Figure 5 (b), illustrates the light colors produced by distinct excitation wavelengths. The diagram displays that the color and chromaticity coordinates (x, y) may be tuned from red ((0.6410, 0.3157) and (0.6205, 0.3346)), thought orange ((0.50411, 0.41414) and (0.4377, 0.4025)) to green (0.3619, 0.4811).

CONCLUSION

In this work, we have reported an investigation of the unusual photoluminescence, $Ln^{3+}\rightarrow Ln^{3+}$ energy transfer and color tuning of a Lanthanide-Organic Framework family. Compound **(2)** is the first example of a LnMOF (MOF) material where the $Ln^{3+}(1)$—$Ln^{3+}(2)$ interaction is strong enough to induce a singular spectral signature.This is quite satisfactorily described theoretically, and our conclusion points to a complex system which properties are controlled by the first coordination sphere geometry in a lanthanide containig MOF. Compound **(3)** shows a green emission with a q = 14%. The emission spectra of **(4)** displays

characteristic narrow bands corresponding to the centered Eu^{3+} $^5D_0 \rightarrow {}^7F_j$ and Tb^{3+} $^5D_4 \rightarrow {}^7F_j$ transitions. The experimental and theoretical ET rates are in good agreement, being predominantly controlled by the *D—Q* and *Q—Q* mechanisms. The emission by compound **(4)** has presented a sensible dependence on the excitation wavelength, enabling an efficient tuning of the photoluminescence color.

SUPPORTING INFORMATION

Calculated solid-state structures, experimental procedures, crystallographic data, lifetime decay curves, time-resolved emission spectra, TGA curves and infrared spectra are included in the supporting information. This material is available free of charge via internet at http://pubs.rsc.org.

AUTHOR INFORMATION

Corresponding author footnote.

* Prof. Dr. Marcelo O. Rodrigues (*marcelozohio@unb.br*), *LIMA-Laboratório de Inorgânica e Materiais, Campus Universitário Darcy Ribeiro, CEP 70904970, P.O.Box 4478, Brasilia-DF, Brazil.* Fax: (+) 55 (61) 32734149; Phone (+)55 (61) 31073867

* Prof. Dr. Claudia Wickleder (wickleder@chemie.uni-siegen.de), *Inorganic Chemistry, Department of Science and Technology, University of Siegen, Siegen 57068, Germany.*

* Prof. Dr. Ricardo Oliveira Freire (*rfreire@ufs.br*), *Pople Computational Chemistry Laboratory, Universidade Federal de Sergipe, 49100-000, São Cristóvão, Sergipe, Brazil.*

AKNOWLEDGEMENT

The authors gratefully acknowledge CNPq (INCT/INAMI and RH-INCT/INAMI), DPP-UNB. FAP-DF, FACEPE (APT-0859—1.06/08), FAPITEC/SE and CAPES for its financial support.

REFERENCES

1. Y. Cui, Y. Yue, G. Qian and B. Chen, *Chem. Rev.*, 2012, **112**, 1126-1162.

2. C. Wang, T. Zhang and W. Lin, *Chem. Rev.*, 2011, **112**, 1084-1104.

3. B. Chen, L. Wang, Y. Xiao, Frank R. Fronczek, M. Xue, Y. Cui and G. Qian, *Angew. Chem., Int. Ed.*, 2009, **48**, 500-503.

4. B. V. Harbuzaru, A. Corma, F. Rey, P. Atienzar, J. L. Jorda, H. Garcia, D. Ananias, L. D. Carlos and J. Rocha, *Angew. Chem., Int. Ed.*, 2008, **47**, 1080-1083.

5. F. Pellé, P. Aschehoug, S. Surblé, F. Millange, C. Serre and G. Férey, *J. Solid State Chem.*, 2010, **183**, 795-802.

6. K. M. L. Taylor, A. Jin and W. B. Lin, *Angew. Chem., Int. Ed.,* 2008, **47**, 7722-7725.

7. I. T. Weber, A. J. Geber de Melo, M. A. de Melo Lucena, M. O. Rodrigues and S. Alves Junior, *Anal. Chem.*, 2011, **83**, 4720-4723.

8. I. T. Weber, I. A. A. Terra, A. J. G. de Melo, M. A. d. M. Lucena, K. A. Wanderley, C. d. O. Paiva-Santos, S. G. Antonio, L. A. O. Nunes, F. A. A. Paz, G. F. de Sa, S. A. Junior and M. O. Rodrigues, *RSC Adv.*, 2012, **2**, 3083-3087.

9. F. A. Almeida Paz, J. Klinowski, S. M. F. Vilela, J. P. C. Tome, J. A. S. Cavaleiro and J. Rocha, *Chem. Soc. Rev.*, 2012, **41**, 1088-1110.

10. Y. Cui, Y. Yue, G. Qian and B. Chen, *Chem. Rev.*, 2012, **112**, 1126-1162.

11. J. Rocha, L. D. Carlos, F. A. Almeida Paz and D. Ananias, *Chem. Soc. Rev.*, 2011, **40**, 926-940.

12. K. Binnemans, *Chem. Rev.*, 2009, **109**, 4283-4374.

13. K. Binnemans and C. GorllerWalrand, *J. Rare Earth.,* 1996, **14**, 173-180.

14. V. E. Karasev, N. V. Petrochenkova, A. G. Mirochnik, M. V. Petukhova and L. I. Lifar, *Rus. J. Coord. Chem.*, 2001, **27**, 746-750.

15. D. Ananias, F. A. Almeida Paz, L. D. Carlos, C. F. G. C. Geraldes and J. Rocha, *Angew. Chem., Int. Ed.*, 2006, **45**, 7938-7942.

16. J. Zhao, L.-S. Long, R.-B. Huang and L.-S. Zheng, *Dalton Trans.*, 2008, **0**, 4714-4716.

17. B. Ay, E. Yildiz, J. D. Protasiewicz and A. L. Rheingold, *Inorg. Chim. Acta*, 2013, **399**, 208-213.

18. L. Pan, X. Y. Huang, J. Li, Y. G. Wu and N. W. Zheng, *Angew. Chem., Int. Ed.*, 2000, **39**, 527-530.

19. K. F. Kelly and W. E. Billups, *Acc. Chem. Res.*, 2012, **46**, 4-13.

20. O. L. Malta, W. M. Azevedo, E. A. Gouveia and G. F. de Sá, *J. Lumin.*, 1982, **26**, 337-343.

21. H. Wen, G. Jia, C.-K. Duan and P. A. Tanner, *PCCP*, 2010, **12**, 9933-9937.

22. M. Tanaka, G. Nishimura and T. Kushida, *Phys. Rev. B*, 1994, **49**, 16917-16925.

23. B. G. W. a. L. Smentek, *Optical Spectroscopy of Lanthanides: Magnetic and Hyperfine Interactions*, CRC Press, Boca Raton, 2007, p. 333, 2007.

24. X. Y. Chen and G. K. Liu, *Journal of Solid State Chemistry*, 2005, **178**, 419-428.

25. P. C. R. Soares-Santos, L. s. Cunha-Silva, F. A. A. Paz, R. A. S. Ferreira, J. o. Rocha, T. Trindade, L. s. D. Carlos and H. I. S. Nogueira, *Cryst. Growth Des.*, 2008, **8**, 2505-2516.

26. J. Legendziewicz, V. Tsaryuk, V. Zolin, E. Lebedeva, M. Borzechowska and M. Karbowiak, *New J. Chem.*, 2001, **25**, 1037-1042.

27. X. Huang, H. Sun, J. Dou, D. Li, D. Wang and G. Liu, *J. Coord. Chem.*, 2007, **60**, 2045-2050.

28. W. Huang, D. Wu, P. Zhou, W. Yan, D. Guo, C. Duan and Q. Meng, *Cryst. Growth Des.*, 2009, **9**, 1361-1369.

29. F. Le Natur, G. Calvez, C. Daiguebonne, O. Guillou, K. Bernot, J. Ledoux, L. Le Pollès and C. Roiland, *Inorg. Chem.*, 2013, **52**, 6720-6730.

30. D. Ananias, M. Kostova, F. A. A. Paz, A. N. C. Neto, R. T. De Moura, O. L. Malta, L. D. Carlos and J. Rocha, *J. Am. Chem. Soc.*, 2009, **131**, 8620-8626.

31. B. R. Judd, *Phys. Rev.*, 1962, **127**, 750-761.

32. G. S. Ofelt, *J. Chem. Phys.*, 1962, **37**, 511-520.

33. O. L. Malta, M. A. C. dosSantos, L. C. Thompson and N. K. Ito, *J. Lumin.*, 1996, **69**, 77-84.

34. J. D. L. Dutra, J. W. Ferreira, M. O. Rodrigues and R. O. Freire, *J. Phys. Chem. A*, 2013, **117**, 14095-14099.

35. H. Peng and J. Travas-Sejdic, *Chem. Mater.*, 2009, **21**, 5563-5565.

36. M. O. Rodrigues, F. A. Paz, R. O. Freire, G. F. de Sá, A. Galembeck, M. C. Montenegro, A. N. Araújo and S. Alves, *J. Phys. Chem. B*, 2009, **113**, 12181-12188.

37. M. O. Rodrigues, N. B. da Costa, C. A. de Simone, A. A. S. Araújo, A. M. Brito-Silva, F. A. A. Paz, M. E. de Mesquita, S. A. Júnior and R. O. Freire, *J. Phys. Chem. B*, 2008, **112**, 4204-4212.

38. R. A. Sá Ferreira, S. S. Nobre, C. M. Granadeiro, H. I. S. Nogueira, L. D. Carlos and O. L. Malta, *J. Lumin.*, 2006, **121**, 561-567.

39. D. T. de Lill, A. de Bettencourt-Dias and C. L. Cahill, *Inorg. Chem.*, 2007, **46**, 3960-3965.

40. T.-F. Liu, W. Zhang, W.-H. Sun and R. Cao, *Inorg. Chem.*, 2011, **50**, 5242-5248.

41. X.-Q. Zhao, X.-H. Liu, J.-J. Li and B. Zhao, *CrystEngComm*, 2013, **15**, 3308-3317.

42. N. Henry, S. Costenoble, M. Lagrenee, T. Loiseau and F. Abraham, *CrystEngComm*, 2011, **13**, 251-258.

43. Y.-H. Zhang, X. Li and S. Song, *Chem. Commun.*, 2013, **49**, 10397-10399.

44. C. Görller-Walrand and K. Binnemans, in *Handbook on the Physics and Chemistry of Rare Earths*, eds. Karl A. Gschneidner, Jr. and E. LeRoy, Elsevier, 1998, vol. Volume 25, pp. 101-264.

45. O. L. Malta, *J. Non-Cryst. Solid.*, 2008, **354**, 4770-4776.

46. T. Kushida, *J. Phys. Soc. Jpn*, 1973, **34**, 1334-1337.

47. T. Kushida, *J. Phys. Soc. Jpn*, 1973, **34**, 1327-1333.

48. T. Kushida, *J. Phys. Soc. Jpn*, 1973, **34**, 1318-1326.

49. S. Edvardsson and M. Klintenberg, *J. Alloy. Comp.*, 1998, **275**, 230-233.

50. W. M. Faustino, O. L. Malta and G. F. de Sá, *J. Chem. Phys.*, 2005, **122**, 054109-054101 - 054109-054110.

51. F. S. T. P.A. Santa-Cruz, *Spectra Lux Software v.2.0, Ponto Quântico Nanodispositivos, UFPE*, 2003.

52. V. Misra and H. Mishra, *J. Chem. Phys.*, 2007, **127**, -.

53. M. J. Weber, *Phys. Rev. B*, 1971, **4**, 2932-2939.

54. R. M. Supkowski and W. D. Horrocks Jr, *Inorg. Chim. Acta*, 2002, **340**, 44-48.

55. Y.-P. Sun, B. Zhou, Y. Lin, W. Wang, K. A. S. Fernando, P. Pathak, M. J. Meziani, B. A. Harruff, X. Wang, H. Wang, P. G. Luo, H. Yang, M. E. Kose, B. Chen, L. M. Veca and S.-Y. Xie, *J. Am. Chem. Soc.*, 2006, **128**, 7756-7757.

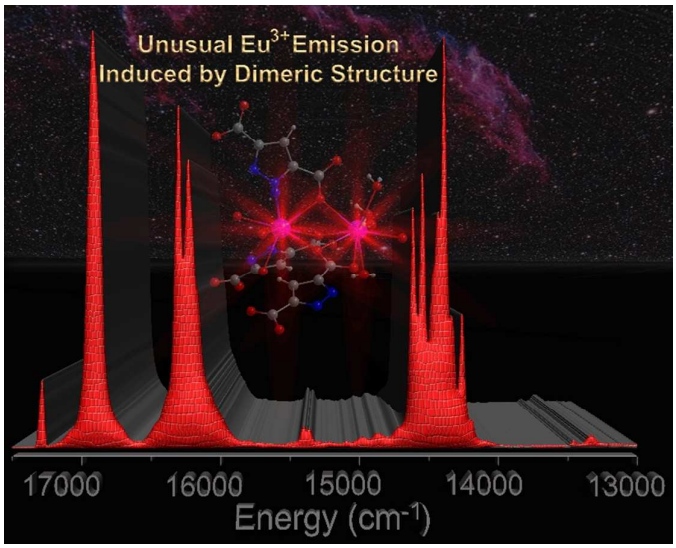

Experimental and theoretical investigation of the spectroscopic properties of four isostructural 3D Ln MOFs shows that their singular photophysical properties are induced by strong interaction between the Ln^{3+} ions.